Graphene oxide adsorption enhanced by *in situ* reduction with sodium hydrosulfite to remove acridine orange from aqueous solution

Ling Sun, Hongwen Yu, Bunshi Fugetsu*

Laboratory of Environmental Remediation, Graduate School of Environmental Science, Hokkaido University, Sapporo 060-0810, Japan

*Corresponding author. E-mail: hu@ees.hokudai.ac.jp.

Telephone/fax: +81-11-706-2272

Abstract

Graphene oxide (GO) is a highly effective adsorbent, and its absorbing capability is further enhanced through its *in situ* reduction with sodium hydrosulfite as the reductant. Acridine orange is the selected target to eliminate with GO as the adsorbent. Under identical conditions, GO without the *in situ* reduction showed a maximum adsorption capacity of 1.4 g g^{-1}, and GO with the *in situ* reduction provided a maximum adsorption capacity of 3.3 g g^{-1}. Sodium hydrosulfite converts carbonyl groups on GO into hydroxyl groups, which function as the key sites for the adsorption enhancement.

Keywords

Graphene oxide, Sodium hydrosulfite, Acridine orange, *In situ* reduction, Hydrogen bonding interaction

1. Introduction

Adsorption is commonly considered to be a fast and relatively technology for water treatment [1]. It normally occurs via both physical and chemical pathways, like activated carbon, which offers the advantage of its porous structure and surface-modified functionalities. Similarly, graphene, consisting of 2D hexagonal lattices of sp^2 carbon atoms covalently bonded, has been theorized to have a huge specific surface area (over 2600 $m^2 g^{-1}$) [2, 3], leading to its potential in the environmental field as an effective choice for pollutant elimination or environmental remediation. Many problems nevertheless remain to be solved before the massive production of graphene for scaled use. However, to date, chemically derived graphene oxide (GO) from graphite has revealed a variety of potential uses because of its flexibility and relatively cheap fabrication. Like a graphene precursor, a subsequent GO reduction could restore the sp^2 carbon structure via various methods such as annealing [4], solvothermal/hydrothermal processes [5-7], or different kinds of reductants [8-15]. However, compared to mechanical exfoliation, functionalities (as defects) can be meanwhile imperfectly introduced onto graphene sheet surfaces. On the other hand, an oxygenation/reduction process confers on GO features that not only are relevant for applications in electrochemistry, such as hybrid materials [16], ultra-capacitors [3, 17], transparent/conducting film [10, 15, 18-21], battery electrodes [22], and sensors [23-25], but that also carry potential in the bioengineering arena. Hu *et al*. reported that graphene-based

materials, i.e., GO or reduced GO paper, showed an excellent inhibitory effect on bacterial growth with mild cytotoxicity [26]. Very recently, Gao *et al*. [27] developed a surface-modified GO mixed with sand for engineered water purification.

Of note, lipophilicity to some extent hinders graphene from being an ideal water-soluble adsorbent. By contrast, however, GO is rich in as-generated oxygen-containing groups, such as hydroxyl and epoxide (mostly located on the top and bottom surfaces), and carboxyl and carbonyl (mostly at the sheet edges), randomly distributed in the graphene structure [28]. Previous work has indicated its application for contaminant removal as a GO/composite. Yang *et al*. demonstrated methylene blue removal by GO with a large adsorption capacity, as high as 714 mg g^{-1} (better than activated carbon, yet less comparable to teak wood bark, with its capacity of 914.6 mg g^{-1}) [29]. Yang *et al.* applied the Cu^{2+}-inducing GO folding/aggregation for ion elimination from aqueous solution, demonstrating an adsorption capacity about 10 times better than that for activated carbon [30]. Other inorganic cations, such as Mg^{2+}, Ca^{2+} [30] and some organic cations, such as methylene blue and malachite green [31] were also found to be capable of folding and/or aggregating GO, because of the electrostatic interactions.

In most previous investigations, researchers have elected to prepare film-like GO/composites and to use reduction to improve electrical conductance. In contrast, here we have directly added the reductant to the GO solution and found that GO folded/aggregated similarly to Cu^{2+}, simultaneously with darkening color. With the large adsorptive capacity of GO, a combination with simultaneous *in situ* reduction

would be another option for environmental application. Recently, Ai *et al*. [32] reported the removal of methylene blue with Fe_3O_4/reduced GO using solvothermal treatment. That work was quite different from the current work in that their simultaneous reduction was performed at the stage of materials preparation while here we performed GO reduction during adsorption. Thereafter, we performed competitive comparisons indicating that sodium hydrosulfite [15] was a highly effective reductant as well as being relatively environmentally friendly, so it was chosen as the reductant. We selected acridine orange (AO) as a target contaminant because it is cell permeable and capable of interacting with DNA and RNA. Adsorption tests were conducted with results clearly demonstrating that with the described treatment, the adsorption capacity and the removal efficiency were dramatically increased compared to as-prepared GO and previous reports. Model fitting of the isotherms indicated that the adsorption implied a Langmuir monolayer behavior. The maximum adsorption reached an unprecedented 3.3 g g^{-1}, compared to as-prepared GO (1.4 g g^{-1}). We also discussed a possible mechanism for the enhancement, combined with various characterizations, inferring that carbonyl group reduction by sodium hydrosulfite was the key to the relatively increased adsorption.

2. Materials and methods

2.1. Materials and reagents

Purified natural graphite was purchased from Bay Carbon, Inc., Michigan, USA. Other chemicals unless noted were from Wako Pure Chemical Industries, Ltd., or Sigma-Aldrich Inc., Japan.

2.2. Preparation of GO

GO was obtained following a modified Hummers-Offeman method [15, 33]. Briefly, graphite (2.0 g), sodium nitrate (1.0 g), concentrated sulfuric acid (98%, 50 mL), and potassium permanganate (6.0 g) were consistently mixed in an ice bath for 2 hours, with the mixture gradually becoming pasty and black-greenish. Next, the mixture was placed in a 35°C water bath and kept at that temperature for 30 minutes, followed by the slow addition of distilled water (100 mL) to keep the solution from effervescing; the resulting solution was placed at well below 100°C for 3 hours. With progression of the reaction, the color turned a little yellowish. After further treatment with H_2O_2 (5%, 100 mL), the filtered cake was washed with distilled water several times until its supernatant was without SO_4^{2-}, as tested using barium chloride (0.1 mM). Then the cake was dispersed in water for further ultra-sonication for 1 hour. Of note, for facilitating the following experiments, we selected solutions with GO centrifuged at speeds ranging from 2000 to 5000 rpm, with a concentration and pH value of approximately 0.48% and 3.1, respectively.

2.3. Adsorption procedure

Time-dependent adsorption tests were conducted in batch mode. Experiments without pH adjustment were carried out at room temperature in tubes containing 50-mL AO at 0.1 g L^{-1} and 1.0 mL GO that was either reduced by sodium hydrosulfite (0.2 g mL^{-1}) added at the 15^{th} minute during the adsorption (GO with such *in situ* reduction, designated as SRGO) or pre-reduced overnight at room temperature (designated as LRGO), respectively. The control (CRTL) groups containing AO and sodium hydrosulfite were set for comparison. The adsorption reaction tubes were agitated at 300 rpm for 180 min to achieve equilibrium. Furthermore, we developed another SRGO control in which GO was pre-reduced for three hours by sodium hydrosulfite, similarly to LRGO (designated as SGRO').

Concentration-dependent experiments were also carried out at room temperature with different starting AO concentrations. AO was prepared with 1.0 g L^{-1}, and then serially diluted by 10, 20, 50, 80, 100, and 200 times, designated as ×10, ×20, ×50, ×80, ×100, and ×200, respectively. These experiments were performed with only SRGO and GO. Both the initial and equilibrium concentrations were recorded for further analysis.

All samples (each 1.5 mL) were centrifuged at 14000 rpm for 10 minutes. The supernatant was measured using a UV-Vis spectrophotometer (JASCO V-570 spectrophotometer) at a wavelength of 492 nm corresponding to the standard curve. All experiments were performed in triplicate, and data are

presented as mean ± SD (standard deviation). The removal efficiency and adsorption capacity were calculated with the following equations:

$$\text{Removal efficiency} = \frac{(C_0 - C_e)}{C_0} \times 100\% \quad (1)$$

$$\text{Adsorption capacity} = \frac{(C_0 - C_e) \times V}{m} \quad (2)$$

Where C_0 (g L^{-1}) and C_e (g L^{-1}) are the initial concentration and equilibrium concentration for AO, respectively, and V (mL) and m (g) indicate the total volume and mass value of adsorbents used, respectively.

2.4. Characterizations

GO-based samples were characterized using various techniques such as atomic force microscopy (AFM, Agilent series 5500 AFM instrument using the tapping mode at a scanning rate of 0.5 Hz), Raman spectroscopy (Raman, an inVia Raman microscope, Renishaw, with an excitation wavelength at 532 nm), Fourier transform infrared spectroscopy (FTIR, FT/IR-6100 FT-IR Spectrometer, JASCO), scanning electronic microscopy (SEM, JSM-6300, JOEL, with acceleration voltage of 30 kV), X-ray photoelectron spectroscopy (XPS, JPC-9010MC, JOEL, using Mg Kα radiation, 1253.6 eV with vacuum better than 1×10^{-7} Torr), and thermo-gravity analysis (TGA, TG/DTA 6200, SII Exstar6000, with a temperature increment of 5°C per minute).

3. Results and discussion

3.1. Graphene oxide and reductants

As mentioned in the experimental section, a modified Hummers method [15] was employed to oxidize and exfoliate graphite into GO. Diluted GO was coated onto freshly exfoliated mica to dry in ambient atmosphere for AFM measurement. As shown in Figure 1, overlapped single layered sheets are clearly identifiable with a thickness of about 0.9 nm. The heavy oxidative process grafted oxygen-containing groups onto the graphene planar surface, enabling development of hydrophilic yet thickened GO sheets (over 0.37 nm [34]). As noted, we especially chose sheets centrifuged between 2000 and 5000 rpm so that large-area GO were easily obtained (Fig. 1). In contrast to smaller pieces, larger sheets could be more easily precipitated because of their heavier molecular weight [35, 36] when undergoing centrifugation, yielding a clean supernatant for sampling.

Considering conventional environmental constraints, we opted for reductants that were highly effective at room temperature. L-ascorbic acid, also known as Vitamin C [9], sodium borohydride [37], and sodium hydrosulfite [15] were selected as candidates because of reducing effects comparable to hydrazine [38]. Figure 2 shows the results of simple tests of these reductants at room temperature. The reaction between sodium borohydride and water produced a soda water–like effervescence. This hydrolysis of sodium

borohydride resulted in decreased reduction efficiency [8]. For sodium hydrosulfite, however, a rapid darkening that appeared with its addition demonstrated its high effectiveness. Instantly, GO pieces became more visible and evenly distributed in the sample. As the reaction progressed over 20 minutes, a clear residual liquid was observed. Meanwhile, the GO sheets aggregated and precipitated at/around the cell wall. There was less change for sodium borohydride and no observable change for L-ascorbic acid, indicating that these reductants would not suit the goals of our applications.

To confirm the reduction with sodium hydrosulfite, analyses with optical microscopy and of the Tyndall scattering effect were conducted. Figure 3 illustrates the morphological changes in GO during the reduction, and Figure 4 provides an indirect representation of the varying GO sizes and hydrophilicity changes. Fewer layered graphene sheets in the GO solution were optically identified because of a rather weak contrast with the surroundings [39]. However, multilayered sheets with some crumples/ripples were occasionally found. The results with the Tyndall effect analysis indicated that GO had a colloidal dispersion. Likewise, the added reductant was observed to darken the sheet color. The change made sheet boundaries clearer, even the fewer-layered sheets (Fig. 3B). Without much delay, head-to-end branch-like GO sheets intertwined/aggregated (Fig. 3C). The formation of large aggregates finally dramatically weakened the Tyndall effect (Fig. 4B). Figure 4C and D show the undoubted hydrophilicity transformation from the reduction, resulting from a decrease in hydrophilic groups on the planar surface and the formation of water-phobic

structures at room temperature [28].

Thus, sodium hydrosulfite is inferred to be a highly effective reagent for GO reduction. Furthermore, hydrosulfite is less toxic, less corrosive and, highly environmentally friendly than some other options, e.g. hydrazine [38] and hydroxylamine hydrochloride [13]. Previous studies have suggested possible mechanisms for the effects of sulfur-containing compounds [8, 9, 15]. We confirmed that the products contained SO_4^{2-} using the $BaCl_2$ method that indicates a positive based on a white precipitate, with findings consistent with those of Chen *et al*. [8]. A possible mechanism involving sodium hydrosulfite is shown as follows, with some modifications of the mechanisms described by Zhou *et al*. [15]:

$$2S_2O_4^{2-} + H_2O \longrightarrow S_2O_3^{2-} + 2HSO_3^- \quad (3)$$

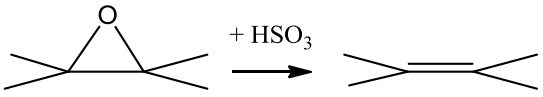

(4)

3.2. Adsorption of GO-based materials

Adsorptions were tested using the GO-based materials. Figure 5 shows the adsorption spectra of the control group (CRTL), which contained only AO and sodium hydrosulfite. The absorbance was recorded at 492 nm, indicating that the reductant did not influence AO [40]. Unless noted specifically, subsequent experiments were carried out using this protocol. A set of images shows the

time-dependent adsorption results for variously treated GO samples with a starting AO concentration of 100 mg g^{-1} (Fig. 6 and Fig. 7). As seen, the discoloration of varying degrees indicates the diverse capacities of adsorbents. Clearly, SRGO had a better decoloration effect than the other samples. A rapid decrease appeared in the initial 10 minutes and then reached the adsorption equilibrium. Based on CTRL, a loss of AO of less than 3% indicated no significant influence of reductants over AO, ensuring the reliability of the adsorption results.

Regarding SRGO, a further decrease occurred to AO once sodium hydrosulfite was added. It increased the removal efficiency to about 95%, the highest of all samples (GO, 67%; LRGO, 76%). This result indicates the generation of more available sites during the *in situ* reduction. However the π-stacking effect counted very little toward adsorption (from graphite, about 3.0 mg g^{-1} with an initial AO concentration of 100 mg g^{-1}). In other words, newly induced functional groups have functioned for AO sorption.

The adsorption capacities were calculated to be 679.5 mg g^{-1}, 976.8 mg g^{-1}, and 781.1 mg g^{-1} for GO, SRGO, and LRGO, respectively. Previous work found that methylene blue had a capacity of up to 714 mg g^{-1} [29]. Thus, GO definitely has proved to have great potential as an adsorbent. In addition, SRGO performed much better than teak wood bark and activated carbon [29]. It is worth noting that a longer pre-reduction period lessened the adsorption capacity, implying that only a suitable reduction degree would maximize the capacity.

Other tests were conducted for SRGO and SRGO' to confirm the superiority of

the *in situ* method. Figure 8 illustrates that SRGO continued to exhibit a better removal performance as well as adsorption capacity in contrast to SRGO', a consistent finding even though SRGO and SRGO' both underwent a three-hour reduction. Analyzing the details for the adsorption progress, given that the reduction degree for GO was no different, required examination of the morphological change in GO sheets. In fact, the pre-reduction partially varied the surface hydrophilicity and resulted in the aggregation of graphene sheets (as similarly reported by Stankovich *et al*. [38]). In addition, the dissolved Na^+ and other ions may have produced a salt effect [36]. As a result, inadequate exfoliation and inaccessible surfaces would appear and induce the adsorption capacity decrease for SRGO' [41]. This scenario could also apply for LRGO.

Here we stress that the amount of the additive GO was halved for SRGO. In other words, GO was diluted twice as much. Nevertheless, its capacity increased to 1382.0 mg g^{-1}, compared to 976 mg g^{-1}, though the removal efficiency decreased to 64% (compared to the previous 95%).

The AO adsorption isotherms on GO and SRGO were then determined as presented in Figure 9. Figure 9A and D demonstrate a positive functional relationship between the adsorption capacity and the equilibrium concentration. The as-obtained capacities were found to be 1255 mg g^{-1} for GO and 2158 mg g^{-1} for SRGO, respectively.

For further understanding the process, Langmuir and Freundlich models were introduced to evaluate the adsorption data. As seen, the equilibrium concentration

(C_e, g L^{-1}) and equilibrium adsorption capacity values (q_e, mg g^{-1}) were fitted by their linearized expressions [29-32, 42-44]. Accordingly, the maximum adsorption capacity for GO and SRGO were calculated by the Langmuir equation, as follows:

$$\text{Langmuir: } \frac{1}{q_e} = \frac{1}{q_m} + \frac{1}{K_L q_m C_e} \quad (5)$$

$$\text{Freundlich: } \ln q_e = \ln K_F + \frac{1}{n} \ln C_e \quad (6)$$

Where, K_L is the Langmuir adsorption constant related to the energy of adsorption (L mg^{-1}); K_F is the Freundlich constant (L mg^{-1}); 1/n is the heterogeneity factor; and q_m is the Langmuir monolayer adsorption capacity (mg g^{-1}).

Figure 9 and Table 1 show the fitting results. The co-efficiency calculated based on the Langmuir model were found to be better than 0.99 for both GO and SRGO; while the co-efficiency calculated based on the Freundlich model were 0.95 for GO and 0.88 for SRGO. The maximum capacities (q_m value) were found to be 1.4 g g^{-1} for GO and 3.3 g g^{-1} for SRGO, respectively.

GO showed a high affinity for positively charged molecules/ions because of oxygen atoms [29-32, 45]. AO is positively charged in nature; accordingly, the electrostatic interaction is the primary binding strength [29]. Because all adsorptions were conducted in weakly acidic conditions (pH 4–5) without pH adjustment, the main interaction between GO and AO relates to the formation of hydrogen bonds [43].

$$\text{-C-OH (GO)} + \text{N-C (AO)} \longrightarrow \text{-C-O-NH-C} \qquad (7)$$

In our work, the adsorption capacity generally negatively relates to the GO additive amount (e.g., for GO, from about 700 to 900 mg g^{-1}). We consider the dilution be an important factor that promotes fully exfoliated GO sheets in the aqueous environment and more access to functional groups as the oxygen functional groups contribute more to adsorption [43, 45, 46]. The SRGO performance involved not only the influence of the dilution but also the functionality changes resulting from the *in situ* reduction.

3.3. Characterizations of GO-based adsorbents and a possible mechanism for the enhancement

It is impressive that SRGO showed the far better adsorption. To uncover more about the mechanism involved, characterizations using SEM, XPS, and FTIR were applied to compare the structures and morphologies of GO before and after reduction. The electric resistivity was measured by a four-probe method as one effective indicator of the extent to which GO was reduced. The GO film obtained by filtration was completely insulating because of the destroyed sp^2-carbon network. By contrast, a simple reduction at room temperature could decrease the resistivity to about 10^4 Ω sq^{-1} (for SRGO and LRGO). This finding indicates partial recovery of GO. Meanwhile, it is obvious that without stricter conditions [7, 13, 15, 46, 47] (e.g., higher temperature), the

reduction is insufficient to maximally improve the conductance.

Figure 10 shows the images of GO/reduced GO by SEM, with direct drying at 80°C. Reference to the scale shows the presence of large GO sheets. More important, for GO, highly ordered structures formed as a result of the semi-ordered accumulation [47] whenever the evaporation/filtration progressed. The interactions of the interlayered hydrogen bonds also were important for facilitating GO sheet adherence to the hydrophilic surfaces [48]. The reduced GO morphologically looks quite different in the image, having become less hydrophilic by reduction. Furthermore, the loss of hydrogen bond donators decreased the inter-layered interactions [28] so that the structures became less compact and more random and crumpled.

Raman spectroscopy is widely used to characterize the structural and electronic properties of GO. It usually involves two main features [12]: a D peak at ~1349 cm^{-1} and a G peak at ~1597 cm^{-1}, arising from the first-order scattering of the E_{2g} phonon of sp^2 C atoms and a breathing mode of k-point photons of A_{1g} symmetry, respectively. Their intensity ratio (I_D/I_G) indicates the degree of the disorder, such as defects, ripples, and edges [49]. Figure 11 reflects our measurement of the reduction degree of each sample at several spots. As shown, the ratios gradually decrease from 2.17 to 1.82. This change could be explained by the average size of the sp^2 domain increasing without the massive creation of new smaller graphitic domains [38]. Coupled with the negligible shifts of the prominent peaks (not shown), room temperature surely is not the best parameter for conductivity restoration by sodium hydrosulfite, which is consistent with the conclusion based on the electric method. Such reduction, however,

may be favorable to the adsorption.

We also employed XPS to analyze GO before and after reduction to observe the evolution of oxygen functional groups, as shown in Figure 12. The reduction degree of GO is described by taking the ratio of C1s to O1s peak areas. As shown in Figure 13A, the C/O ratio increased from 2.67 (GO), to 3.26 (SRGO), and then to 4.09 (LRGO); the prominence of the carbon peak finally replaced the oxygen. It is true that GO underwent a deoxygenation at room temperature. Additionally, the four peaks centered at around 284.4, 286.7, 288.5, and 290.5 eV are assigned to the C(C-H/C-C), C-O(C-OH/C-O-C), C=O, and –COO- groups, respectively (Fig. 13B–D). GO is by nature insulating and thus exhibits the binding energy redshift in C1s spectra (about +0.5 eV here), whereas it does not influence the following analysis. As seen in the figure, the carbon proportion rises from about 5% to 48% from GO to LRGO. More specifically, the intensity of the C-O peak exhibits an increase followed by a decrease, from 48% to 69% and then to 41%; at the same time, the C=O dramatically decreases after the 3-hour reduction (SRGO) from 39% to 5%. It is clear from the figure that the C-O still occupies a large proportion over the long reduction process (LRGO), which indicates that the room temperature *in situ* reduction method could not completely remove the oxygen-containing groups. As the figure illustrates, with the differences between the C-O and C=O proportions, it can be inferred that the adsorption enhancement is probably related to the C=O (carbonyl group). In other words, the increased amount of hydroxyl groups probably results from the reduction of carbonyl

groups.

For further evidence, FTIR was also employed, as shown in Figure 13. The carbonyl groups are ascribed to the band at 1720 cm^{-1}. The bands at around 1053, 1089, and 1233 cm^{-1} are ascribed to the vibration of C-O; the bands at about 2921 and 2855 cm^{-1} are ascribed to the vibration of C-H. Coupled with XPS findings, a common change is notable before and after the reduction. The intensity of C=O is markedly weakened as the C-O/C-H becomes much stronger after reduction. Meanwhile, the C=C peak (at 1625 cm^{-1}) shifted to 1610 cm^{-1}, possibly because of the sp^2 structure restoration. On the spectrum of LRGO in the figure, the C=C peak is rather weak in contrast to that of the C-O (at 1089 cm^{-1}) and C-H. This result demonstrates that the reduction could not restore sp^2 structures to the maximum possible when done at room temperature with sodium hydrosulfite. This result is in agreement with the above conclusions.

As seen in Figure 14, TG-A was also carried out under N_2 atmosphere. Both LRGO (69.3%) and SRGO (45.5%) are much more stable than GO (36.5%), as deduced by their residues. In general, mass loss throughout the procedure normally consists of two major steps, the small amount of inter-lamellar water evaporation as the initial weight loss and the functional group decomposition into gases between the intercalated layers [8]. The former could be used to explain the little peak on the TG-A curve at about 220°C (not shown in Fig. 13) [50], but it was not found in SRGO and LRGO. This distinction implies that the ordered layered structures diminished and were replaced by non-compact structures, as seen in the SEM image of the reduced

GO. Of interest, there was a considerable mass loss at 810°C for SRGO in the combustion curve. It is inferred that stable oxygen-containing groups would have formed, such as hydroxyl groups.

Based on the various characterizations, the carbonyl group turned out to be the origin of hydroxyl groups after the reduction. Sodium hydrosulfite is known to reduce carbonyl groups, as reported by Devries *et al*. [51]. The reaction here at room temperature is described as follows:

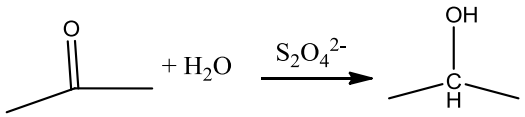

(8)

The carbonyl is reduced by the hydrosulfite, resulting in the formation of C-OH and C-H bonds. Thus, the reduction/decrease of carbonyl groups increases the hydroxyl and hydrocarbon bonds. As the reduction progresses, the dye molecules are absorbed via the hydrogen bond, as described above (Fig. 15). This inference provides a good basis for explaining the change in the characterizations and additional capacity of SRGO.

4. Conclusions

We have developed an enhancement method involving simultaneous *in situ* reduction of GO by $Na_2S_2O_4$, using AO adsorption on GO. An adsorption capacity of GO as high as 2158 mg g^{-1} was obtained by this means, proving to be the best among

other treatments in our work. Meanwhile, the as-prepared GO also effectively removed AO in an aqueous environment. The adsorption capacity of GO could reach up to 1255 mg g^{-1} with the mass fraction of GO at about 0.048‰. As the GO concentration was increased up to two fold, the removal efficiency rose from 64% to 95%, but the capacity decreased to 976 mg g^{-1}. The Langmuir model fitted the adsorption data better than the Freundlich model, indicating a maximum capacity as high as 3.3 g g^{-1} for the *in situ* method, and 1.4 g g^{-1} for GO. Both the adsorptions behave in a monolayer manner, and the exfoliation degree of GO is important for its capacity. We also investigated the mechanism involved in the enhancement. With various characterizations using XPS, FTIR, Raman, and TGA, we found that the reduction of carbonyl groups resulted in hydroxyl groups, which played an important role in the development of the extra-large capacity from our method. This phenomenon may open up a route for environmental applications using GO as an effective adsorbent.

References

[1] I. Ali, V.K. Gupta, Advances in water treatment by adsorption technology, Nat. Protoc., 1 (2006) 2661-2667.

[2] S. Stankovich, D.A. Dikin, G.H.B. Dommett, K.M. Kohlhaas, E.J. Zimney, E.A. Stach, R.D. Piner, S.T. Nguyen, R.S. Ruoff, Graphene-based composite materials, Nature, 442 (2006) 282-286.

[3] M.D. Stoller, S.J. Park, Y.W. Zhu, J.H. An, R.S. Ruoff, Graphene-based ultracapacitors, Nano Lett., 8 (2008) 3498-3502.

[4] C.D. Zangmeister, Preparation and evaluation of graphite oxide reduced at 220 °C, Chem. Mater., 22 (2010) 5625-5629.

[5] S. Dubin, S. Gilje, K. Wang, V.C. Tung, K. Cha, A.S. Hall, J. Farrar, R. Varshneya, Y. Yang, R.B. Kaner, A one-step, solvothermal reduction method for producing reduced graphene oxide dispersions in organic solvents, ACS Nano, 4 (2010) 3845-3852.

[6] D. Long, W. Li, L. Ling, J. Miyawaki, I. Mochida, S.H. Yoon, Preparation of nitrogen-doped graphene sheets by a combined chemical and hydrothermal reduction of graphene oxide, Langmuir, 26 (2010) 16096-16102.

[7] O.C. Compton, B. Jain, D.A. Dikin, A. Abouimrane, K. Amine, S.T. Nguyen, Chemically active reduced graphene oxide with tunable C/O ratios, ACS Nano, 5 (2011) 4380-4391.

[8] W.F. Chen, L.F. Yan, P.R. Bangal, Chemical reduction of graphene oxide to graphene by sulfur-containing compounds, J. Phys. Chem. C, 114 (2010)

19885-19890.

[9] J. Gao, F. Liu, Y.L. Liu, N. Ma, Z.Q. Wang, X. Zhang, Environment-friendly method to produce graphene that employs vitamin C and amino acid, Chem. Mater. , 22 (2010) 2213-2218.

[10] S.F. Pei, J.P. Zhao, J.H. Du, W.C. Ren, H.M. Cheng, Direct reduction of graphene oxide films into highly conductive and flexible graphene films by hydrohalic acids, Carbon, 48 (2010) 4466-4474.

[11] X.F. Gao, J. Jang, S. Nagase, Hydrazine and Thermal Reduction of Graphene Oxide: Reaction Mechanisms, Product Structures, and Reaction Design, J. Phys. Chem. C, 114 (2010) 832-842.

[12] C. Zhu, S. Guo, Y. Fang, S. Dong, Reducing sugar: new functional molecules for the green synthesis of graphene nanosheets, ACS Nano, 4 (2010) 2429-2437.

[13] S. Mao, K. Yu, S. Cui, Z. Bo, G. Lu, J. Chen, A new reducing agent to prepare single-layer, high-quality reduced graphene oxide for device applications, Nanoscale, 3 (2011) 2849-2853.

[14] T.A. Pham, J.S. Kim, J.S. Kim, Y.T. Jeong, One-step reduction of graphene oxide with L-glutathione, Colloid. Surface. A, 384 (2011) 543-548.

[15] T.N. Zhou, F. Chen, K. Liu, H. Deng, Q. Zhang, J.W. Feng, Q.A. Fu, A simple and efficient method to prepare graphene by reduction of graphite oxide with sodium hydrosulfite, Nanotechnology, 22 (2011) 045704.

[16] J.C. Liu, Y.J. Wang, L. Liu, D.D. Sun, High-quality reduced graphene oxide-nanocrystalline platinum hybrid materials prepared by simultaneous

co-reduction of graphene oxide and chloroplatinic acid, Nanoscale Res Lett, 6 (2011) 241.

[17] C. Liu, Z. Yu, D. Neff, A. Zhamu, B.Z. Jang, Graphene-based supercapacitor with an ultrahigh energy density, Nano Lett., 10 (2010) 4863-4868.

[18] M. Zhou, Y.L. Wang, Y.M. Zhai, J.F. Zhai, W. Ren, F.A. Wang, S.J. Dong, Controlled synthesis of large-area and patterned electrochemically reduced graphene oxide films, Chem. Eur. J., 15 (2009) 6116-6120.

[19] B. Li, X.T. Zhang, X.H. Li, L. Wang, R.Y. Han, B.B. Liu, W.T. Zheng, X.L. Li, Y.C. Liu, Photo-assisted preparation and patterning of large-area reduced graphene oxide-TiO2 conductive thin film, Chem. Commun., 46 (2010) 3499-3501.

[20] Y.W. Zhu, W.W. Cai, R.D. Piner, A. Velamakanni, R.S. Ruoff, Transparent self-assembled films of reduced graphene oxide platelets, Appl. Phys. Lett., 95 (2009) 103104.

[21] J. Zhao, S. Pei, W. Ren, L. Gao, H.M. Cheng, Efficient preparation of large-area graphene oxide sheets for transparent conductive films, ACS Nano, 4 (2010) 5245-5252.

[22] X. Xiao, P. Liu, J.S. Wang, M.W. Verbrugge, M.P. Balogh, Vertically aligned graphene electrode for lithium ion battery with high rate capability, Electrochem. Commun., 13 (2010) 209-212.

[23] H.Q. Luo, W.T. Huang, Y. Shi, W.Y. Xie, N.B. Li, A reversible fluorescence nanoswitch based on bifunctional reduced graphene oxide: use for detection of Hg(2+) and molecular logic gate operation, Chem. Commun., 47 (2011) 7800-7802.

[24] J.T. Robinson, F.K. Perkins, E.S. Snow, Z.Q. Wei, P.E. Sheehan, Reduced graphene oxide molecular sensors, Nano Lett., 8 (2008) 3137-3140.

[25] Y.H. Lin, Y.Y. Shao, J. Wang, H. Wu, J. Liu, I.A. Aksay, Graphene based electrochemical sensors and biosensors: a review, Electroanal., 22 (2010) 1027-1036.

[26] W. Hu, C. Peng, W. Luo, M. Lv, X. Li, D. Li, Q. Huang, C. Fan, Graphene-based antibacterial paper, ACS Nano, 4 (2010) 4317-4323.

[27] W. Gao, M. Majumder, L.B. Alemany, T.N. Narayanan, M.A. Ibarra, B.K. Pradhan, P.M. Ajayan, Engineered graphite oxide materials for application in water purification, Acs. Appl. Mater. Inter., 3 (2011) 1821-1826.

[28] S. Stankovich, R.D. Piner, S.T. Nguyen, R.S. Ruoff, Synthesis and exfoliation of isocyanate-treated graphene oxide nanoplatelets, Carbon, 44 (2006) 3342-3347.

[29] S.T. Yang, S. Chen, Y. Chang, A. Cao, Y. Liu, H. Wang, Removal of methylene blue from aqueous solution by graphene oxide, J. Colloid Interf. Sci, 359 (2011) 24-29.

[30] S.T. Yang, Y. Chang, H. Wang, G. Liu, S. Chen, Y. Wang, Y. Liu, A. Cao, Folding/aggregation of graphene oxide and its application in Cu2+ removal, J. Colloid. Interf. Sci., 351 (2010) 122-127.

[31] P. Bradder, S.K. Ling, S.B. Wang, S.M. Liu, Dye adsorption on layered graphite oxide, J. Chem. Eng. Data, 56 (2011) 138-141.

[32] L. Ai, C. Zhang, Z. Chen, Removal of methylene blue from aqueous solution by a solvothermal-synthesized graphene/magnetite composite, J. Hazard. Mater., 192 (2011) 1515-1524.

[33] W.S. Hummers, R.E. Offeman, Preparation of graphitic oxide, J. Am. Chem. Soc., 80 (1958) 1339-1339.

[34] M. Inagaki, Y.A. Kim, M. Endo, Graphene: preparation and structural perfection, J. Mater. Chem., 21 (2011) 3280-3294.

[35] B. Fugetsu, E. Sano, H.W. Yu, K. Mori, T. Tanaka, Graphene oxide as dyestuffs for the creation of electrically conductive fabrics, Carbon, 48 (2010) 3340-3345.

[36] D. Li, M.B. Muller, S. Gilje, R.B. Kaner, G.G. Wallace, Processable aqueous dispersions of graphene nanosheets, Nat Nanotechnol, 3 (2008) 101-105.

[37] H.J. Shin, K.K. Kim, A. Benayad, S.M. Yoon, H.K. Park, I.S. Jung, M.H. Jin, H.K. Jeong, J.M. Kim, J.Y. Choi, Y.H. Lee, Efficient reduction of graphite oxide by sodium borohydrilde and its effect on electrical conductance, Adv. Funct. Mater., 19 (2009) 1987-1992.

[38] S. Stankovich, D.A. Dikin, R.D. Piner, K.A. Kohlhaas, A. Kleinhammes, Y. Jia, Y. Wu, S.T. Nguyen, R.S. Ruoff, Synthesis of graphene-based nanosheets via chemical reduction of exfoliated graphite oxide, Carbon, 45 (2007) 1558-1565.

[39] P. Blake, E.W. Hill, A.H.C. Neto, K.S. Novoselov, D. Jiang, R. Yang, T.J. Booth, A.K. Geim, Making graphene visible, Appl. Phys. Lett., 91 (2007) 063124

[40] H.W. Yu, B. Fugetsu, A novel adsorbent obtained by inserting carbon nanotubes into cavities of diatomite and applications for organic dye elimination from contaminated water, J. Hazard. Mater., 177 (2010) 138-145.

[41] D.R. Dreyer, S. Park, C.W. Bielawski, R.S. Ruoff, The chemistry of graphene oxide, Chem. Soc. Rev. , 39 (2010) 228-240.

[42] Z.J. Fan, W. Kai, J. Yan, T. Wei, L.J. Zhi, J. Feng, Y.M. Ren, L.P. Song, F. Wei, Facile synthesis of graphene nanosheets via Fe reduction of exfoliated graphite oxide, ACS Nano, 5 (2011) 191-198.

[43] T. Hartono, S.B. Wang, Q. Ma, Z.H. Zhu, Layer structured graphite oxide as a novel adsorbent for humic acid removal from aqueous solution, J. Colloid. Interf. Sci., 333 (2009) 114-119.

[44] M.I. Kandah, J.L. Meunier, Removal of nickel ions from water by multi-walled carbon nanotubes, J. Hazard. Mater., 146 (2007) 283-288.

[45] C.J. Zhou, W.J. Zhang, W.C. Zhou, A.H. Lei, Q.L. Zhang, Q. Wan, B.S. Zou, Fast and considerable adsorption of methylene blue dye onto graphene oxide, Bull. Environ. Contam. Toxicol, 87 (2011) 86-90.

[46] N.I. Kovtyukhova, P.J. Ollivier, B.R. Martin, T.E. Mallouk, S.A. Chizhik, E.V. Buzaneva, A.D. Gorchinskiy, Layer-by-layer assembly of ultrathin composite films from micron-sized graphite oxide sheets and polycations, Chem. Mater., 11 (1999) 771-778.

[47] K.W. Putz, O.C. Compton, C. Segar, Z. An, S.T. Nguyen, L.C. Brinson, Evolution of order during vacuum-assisted self-assembly of graphene oxide paper and associated polymer nanocomposites, ACS Nano, 5 (2011) 6601-6609.

[48] M. Chhowalla, G. Eda, Chemically derived graphene oxide: towards large-area thin-film electronics and optoelectronics, Adv. Mater., 22 (2010) 2392-2415.

[49] W. Choi, G.H. Moon, Y. Park, W. Kim, Photochemical loading of metal nanoparticles on reduced graphene oxide sheets using phosphotungstate, Carbon, 49

(2011) 3454-3462.

[50] X. Tong, H. Wang, G. Wang, L.J. Wan, Z.Y. Ren, J.T. Bai, J.B. Bai, Controllable synthesis of graphene sheets with different numbers of layers and effect of the number of graphene layers on the specific capacity of anode material in lithium-ion batteries, J. Solid State Chem., 184 (2011) 982-989.

[51] J.G. Devries, R.M. Kellogg, Reduction of aldehydes and ketones by sodium dithionite, J. Org. Chem., 45 (1980) 4126-4129.

Figures and Captions

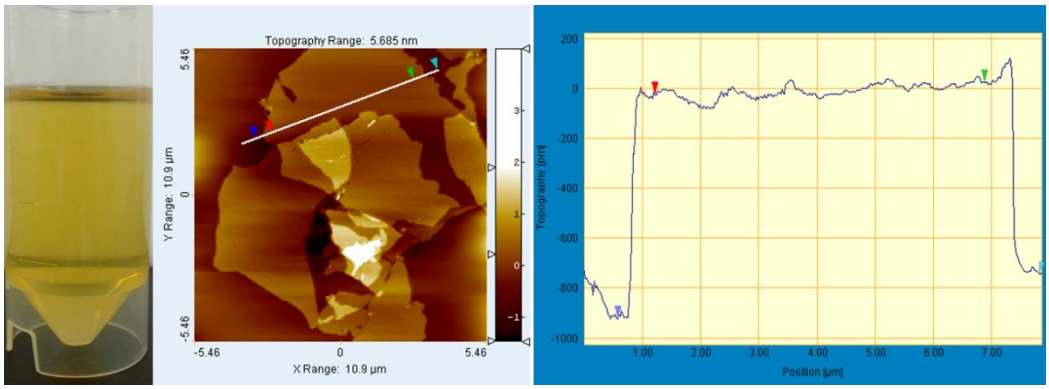

Fig. 1. Digital image of GO solution and a typical AFM image of exfoliated GO on mica (left) with a cross-sectional profile (right) indicating the thickness and width at about 0.9 nm and 6 µm, respectively.

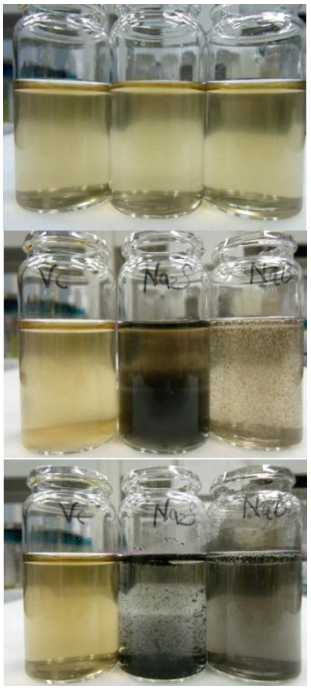

Fig. 2. Images of the GO reduction process with different reductants. Left: L-ascorbic acid; middle: sodium hydrosulfite; right: sodium borohydride.

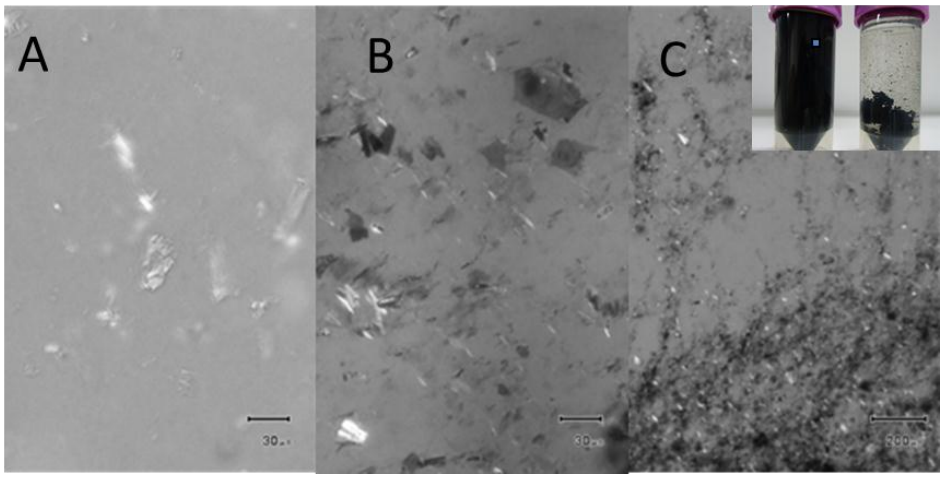

Fig. 3. A series of optical microscopy images showing the aqueous reduction process of GO by the additive $Na_2S_2O_4$. A: GO dispersion containing large pieces of GO sheets (scale bar: 30 μm). B: Color change of GO the instant $Na_2S_2O_4$ was added. C: GO aggregated and precipitated after 24 h (and inset).

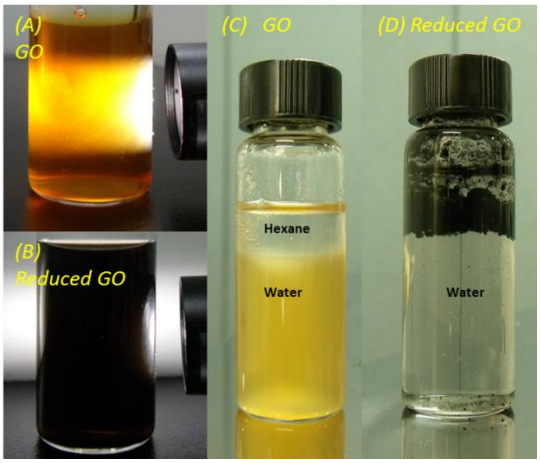

Fig. 4. Tyndall scattering effect of GO (A) and reduced GO (B) with a beam of visible light passing through. C: GO evenly dispersed in water. D: Reduced GO in oil phase (hexane).

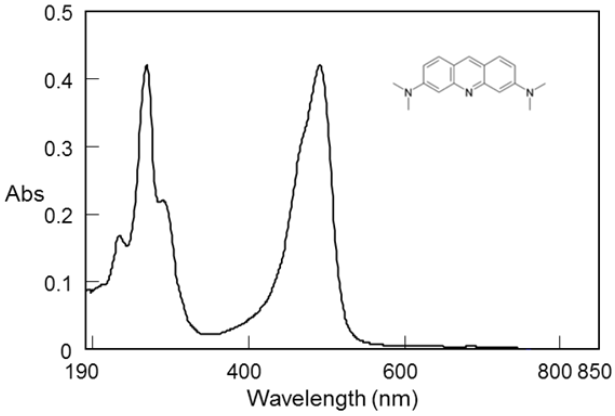

Fig. 5. UV-Vis scanning spectra of AO solution mixed with $Na_2S_2O_4$.

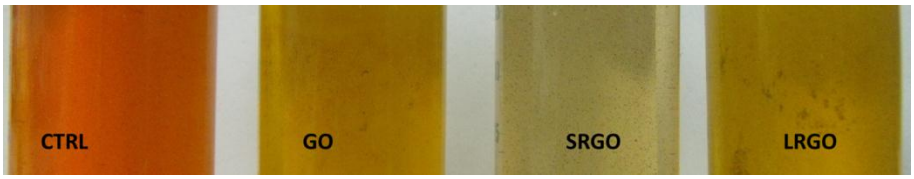

Fig. 6. Digital images of CTRL, GO, SRGO, and LRGO after adsorptions.

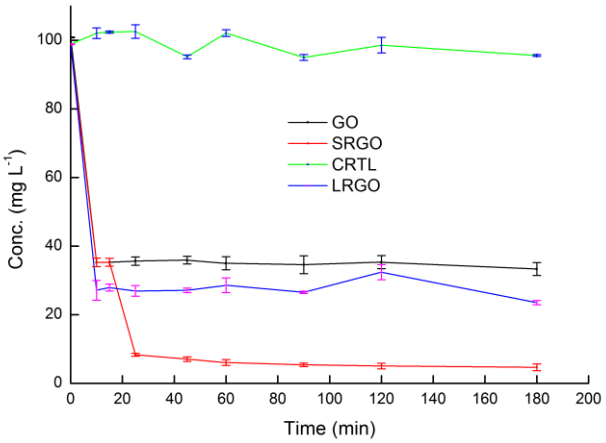

Fig. 7. Time-dependent adsorption of AO (100 mg L^{-1}) with GO, SRGO, and LRGO (Additive amount of GO: 1 mL) compared to AO in reducing solution (CTRL), at room temperature. Note: For SRGO, adsorption was performed with addition of the reductant at the 15th minute (removal efficiency about 95%); for LRGO, GO was pre-treated with reductant overnight at room temperature with removal efficiency of 76%; for GO, removal efficiency was about 67%.

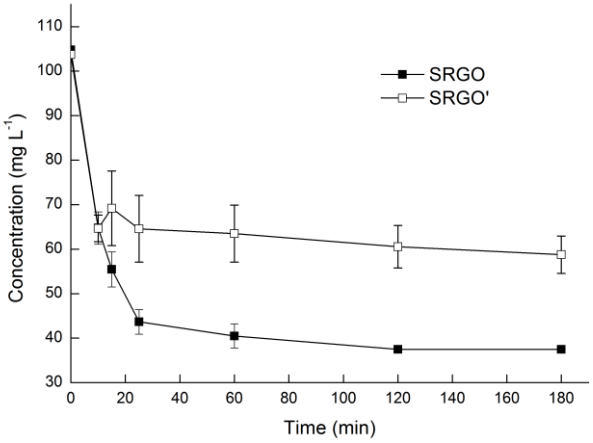

Fig. 8. Time-dependent adsorptions with SRGO and SRGO' (additive amount of GO: 0.5 mL). SRGO': GO was pre-reduced for 3 h.

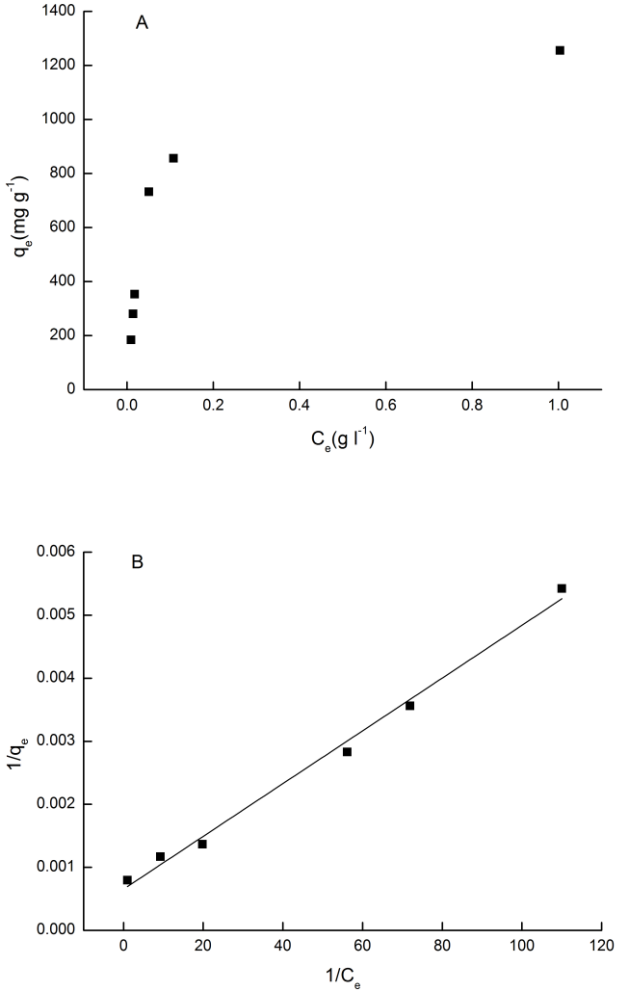

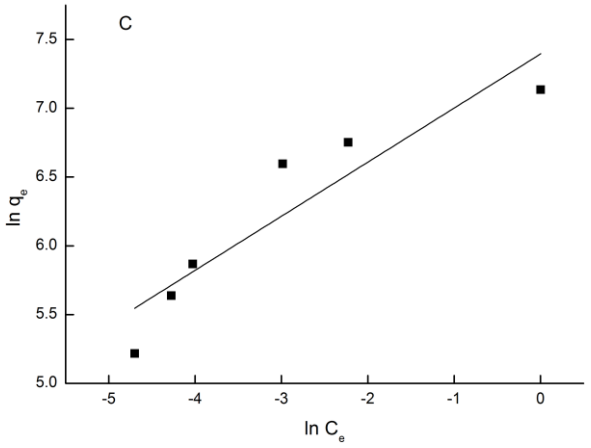
C
7.5
7.0
6.5
6.0
5.5
5.0
ln q_e
-5
-4
-3
-2
-1
0
ln C_e

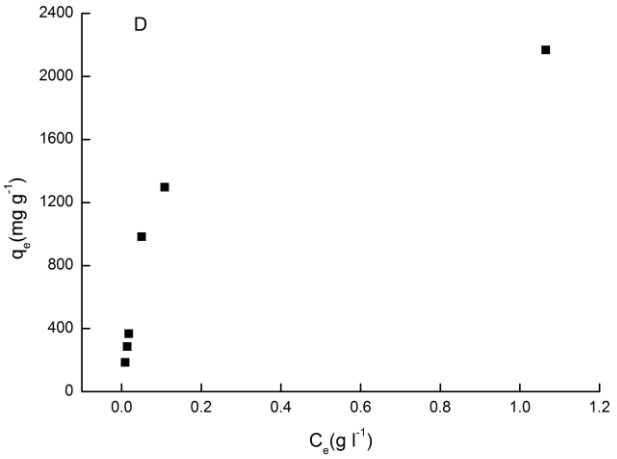
D
2400
2000
1600
1200
800
400
0
q_e(mg g^{-1})
0.0
0.2
0.4
0.6
0.8
1.0
1.2
C_e(g l^{-1})

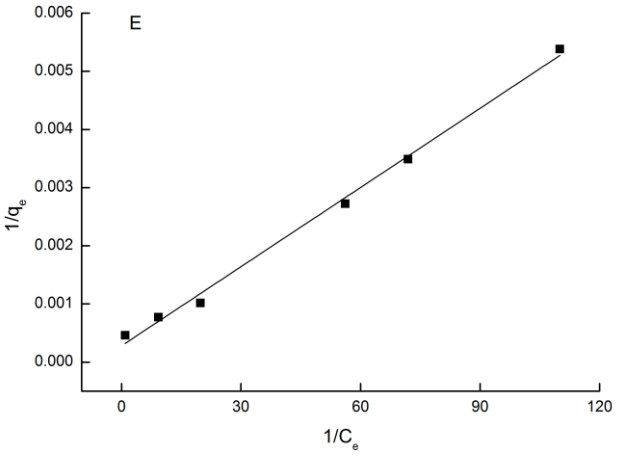
E
0.006
0.005
0.004
0.003
0.002
0.001
0.000
$1/q_e$
0
30
60
90
120
$1/C_e$

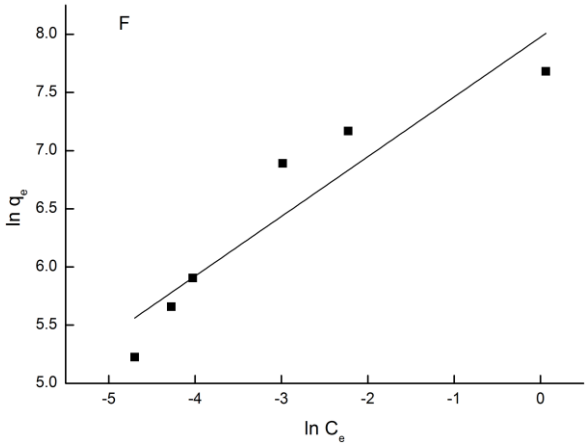

Fig. 9. Adsorption isotherms of GO (A) and SRGO (D), and their results fitted by the Langmuir model (B, E) and the Freundlich model (C, F).

Table 1. The fitting parameters for AO adsorption on GO/SRGO

	Langmuir isotherm			**Freundlich isotherm**		
	K_L **(l mg^{-1})**	q_m **(mg g^{-1})**	R^2	K_f	**n**	R^2
GO	17.5	1428	0.9932	4011	1.59	0.9531
SRGO	6	3333	0.9959	2906	1.95	0.8818

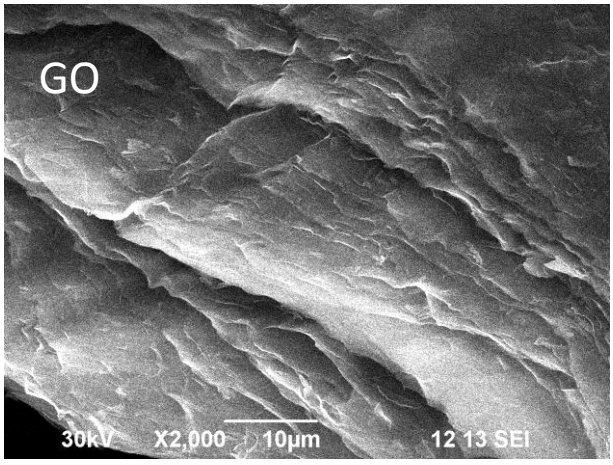

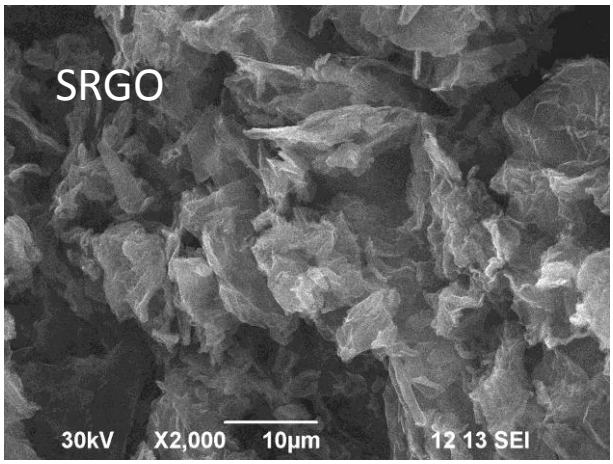

Fig. 10. SEM images of GO (upper) and reduced GO (lower).

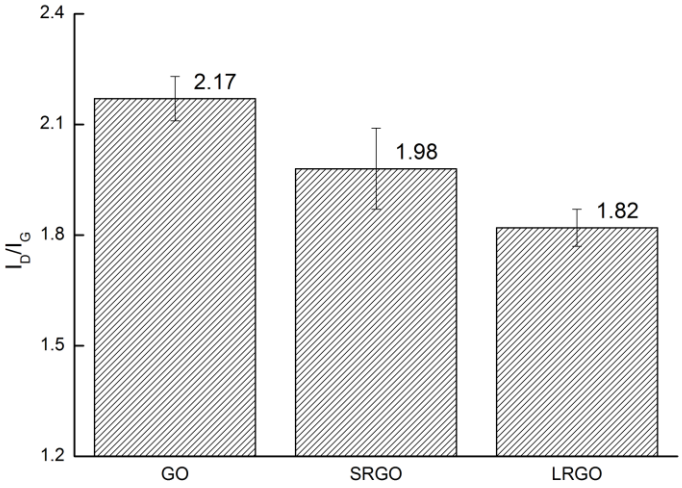

Fig. 11. Histogram of I_D/I_G ratios from Raman spectra of GO, SRGO, and LRGO.

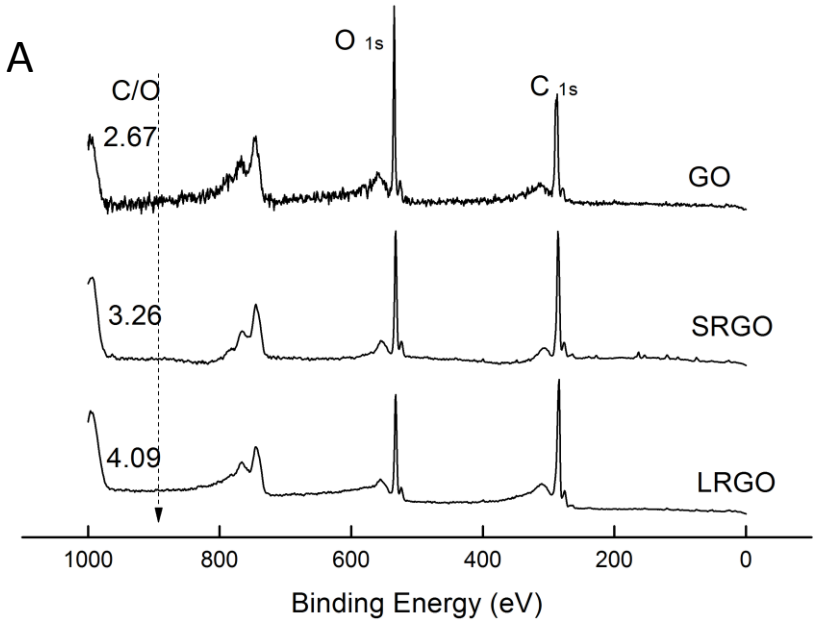
A
O 1s
C 1s
C/O
2.67
GO
3.26
SRGO
4.09
LRGO
1000
800
600
400
200
0
Binding Energy (eV)

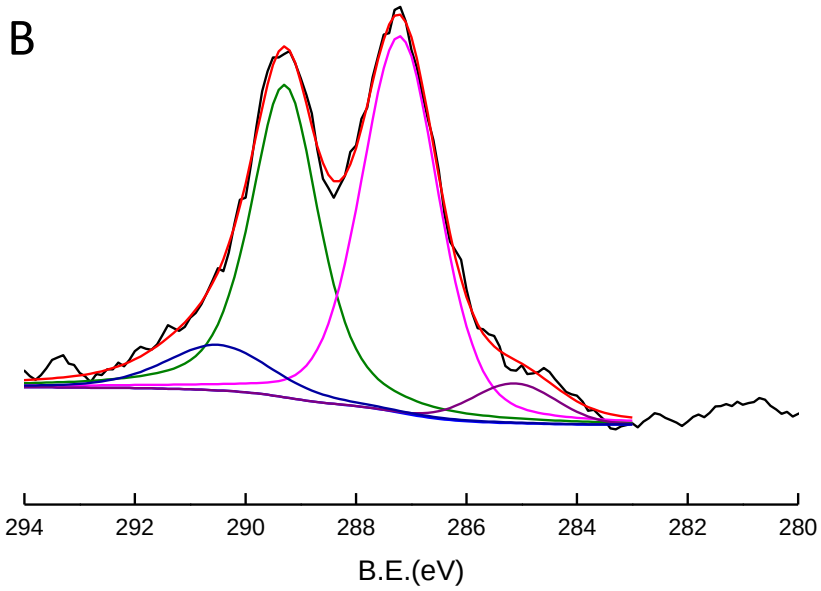
B
294
292
290
288
286
284
282
280
B.E.(eV)

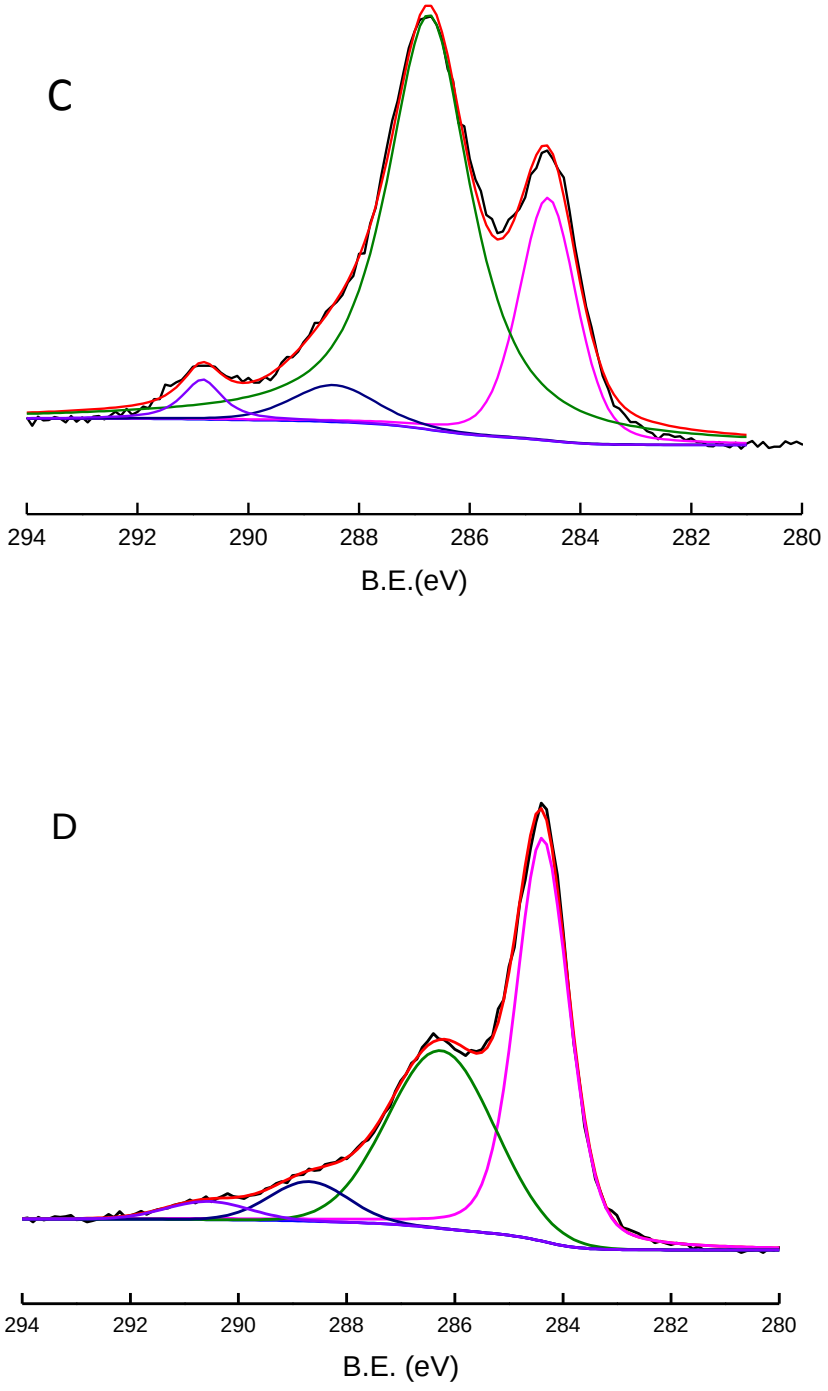

Fig. 12. XPS general spectra and curve fit of C1s spectra of GO, SRGO, and LRGO.

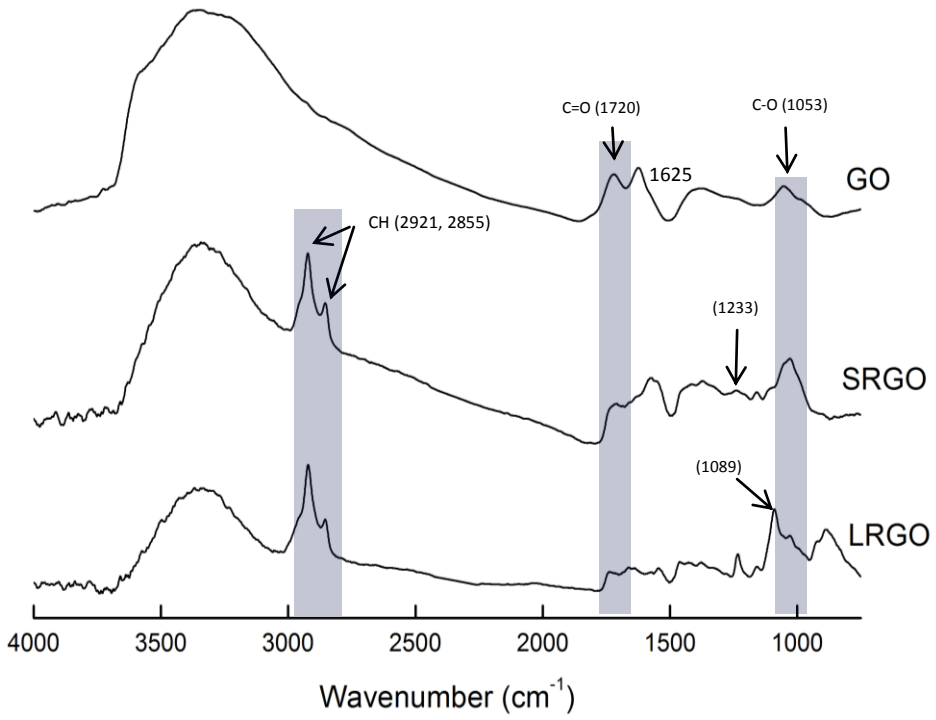

Fig. 13. Fourier transform infrared spectra (*vs.* absorbance) of as-prepared GO, SRGO, and LRGO.

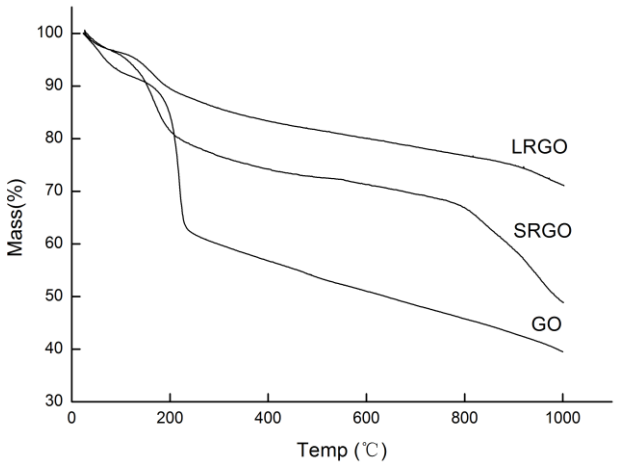

Fig. 14. Thermo-gravimetric analysis for GO, SRGO, and LRGO.

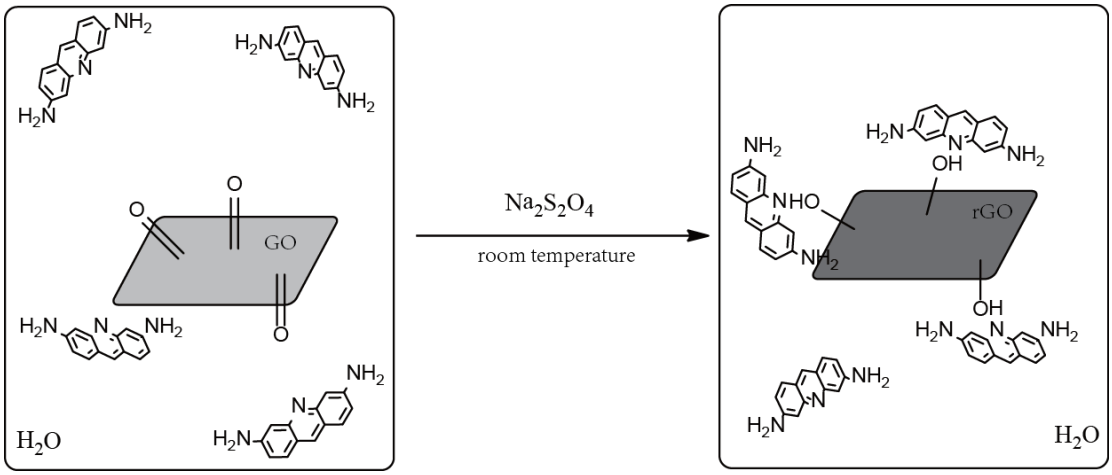

Fig. 15. Possible mechanism for the AO sorption enhancement.